Semiannual Progress Report on Real Time Control for NASA Robotic Gripper

Carole A. Salter and John S. Baras
Electrical Engineering Department
and
Systems Research Center
University of Maryland, College Park

Ending: 2/15/89

February 15, 1989

1 Introduction

Manipulating objects in space presents very different kinds of problems than it does on earth, in fact in many respects it is much more difficult. Accordingly, the design and control of *space manipulators* must reflect these differences. Reaction forces and torques normally damped by the earth, can create problems in space. For instance, an astronaut attempting to turn a valve on a relatively large space vehicle must be securely attached to the vehicle, otherwise, instead of turning the valve, the torque created will serve to turn the astronaut relative to the vehicle. This is by no means the only difficulty. Consider the following scenario: A master slave arm is being used to link beams for a large space structure. The sockets used to link the beams are transported on trays to the locations of the beam joints. Due to the zero gravity environment, the sockets must be fixed in place by some type of fastener to ensure they remain on the tray. Designing the end effector to release the fastener while maintaining a firm grasp on the socket will solve both the problems associated with torques and reaction forces, as well as the problem of minor perturbations dispersing the sockets in random directions.

To accommodate these problems NASA developed the *gripper/nut runner*. The *gripper/nut runner* has two fingers which together have one degree of freedom. Similar to a vice, the width of the opening is the only variable. Centered between the fingers is a device for unscrewing nuts. Having one degree of freedom, this *nut runner* will be actuated by wrist rotations. Pictures of the *gripper*, side, end, and top views, can be found in figures 1, 2, and 3 respectively. Still in the design phase, the *nut runner* is not present in the figures.

This project's aim is to develop control laws (in some optimal sense) for the *gripper/nut runner* end effector. Control laws for the *gripper* and *nut runner* portions of the end effector may be developed independently since these two systems are decoupled. A hybrid force/position controller will be used for both the *gripper* and *nut runner*. Developed here is the *gripper* controller only. Sensory data available to the controller is obtained from an array of strain qauges [1] as well as a linear potentiometer. Applying well known optimal control theoretic principles, the control which minimizes the transition time between positions is obtained. In addition, a robust force control scheme is developed to contend with the strain gauge drift caused by extreme temperature variations encountered in space.

2 Mathematical Model

For analytical purposes it is necessary to establish a mathematical model for the system. This model will include the actuator, transmission mechanism, and finger assembly.

The finger actuator is a permanent-magnet DC motor. Models for these motors can be obtained from various sources. Used here is the model developed in *Modern Control Engineering* [2].

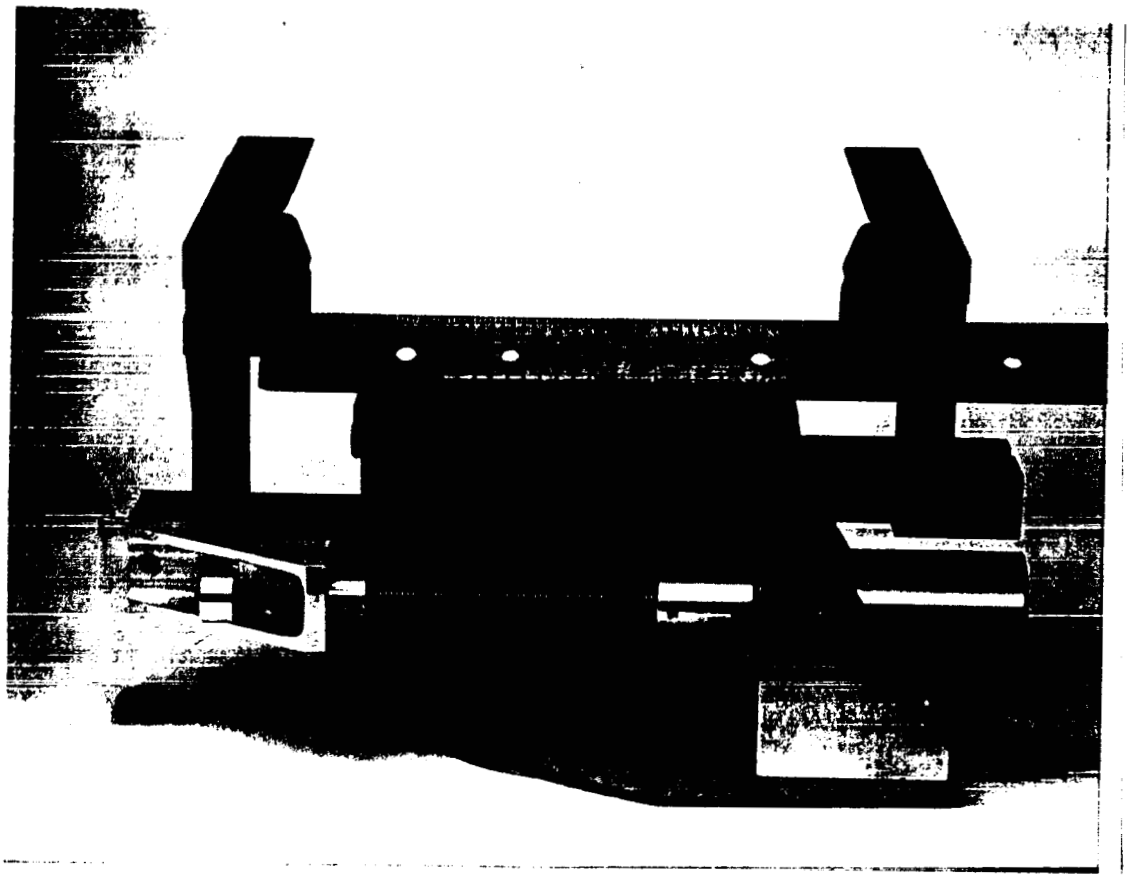

Figure 1: *Gripper (side view)*

The armature is modeled by a resistance R_a, and inductance L_a, both in series with a voltage source e_b representing the back emf generated by the rotor rotations. Applied to the armature terminals is the control voltage e_a.

Proportional to the armature current by a constant k_i, the motor torque is given by

$$T_m(t) = k_i i_a(t). \tag{2.1}$$

Also, the back emf is proportional to the rotor angular velocity by constant k_b,

$$e_b(t) = k_b \omega_m(t). \tag{2.2}$$

The power in the motor armature can be expressed as

$$p = \underline{e_a(t) i_a(t)} \quad (N/s) \tag{2.3}$$

or

$$p = \underline{T_m(t) \omega_m(t)} \quad (N/s) \tag{2.4}$$

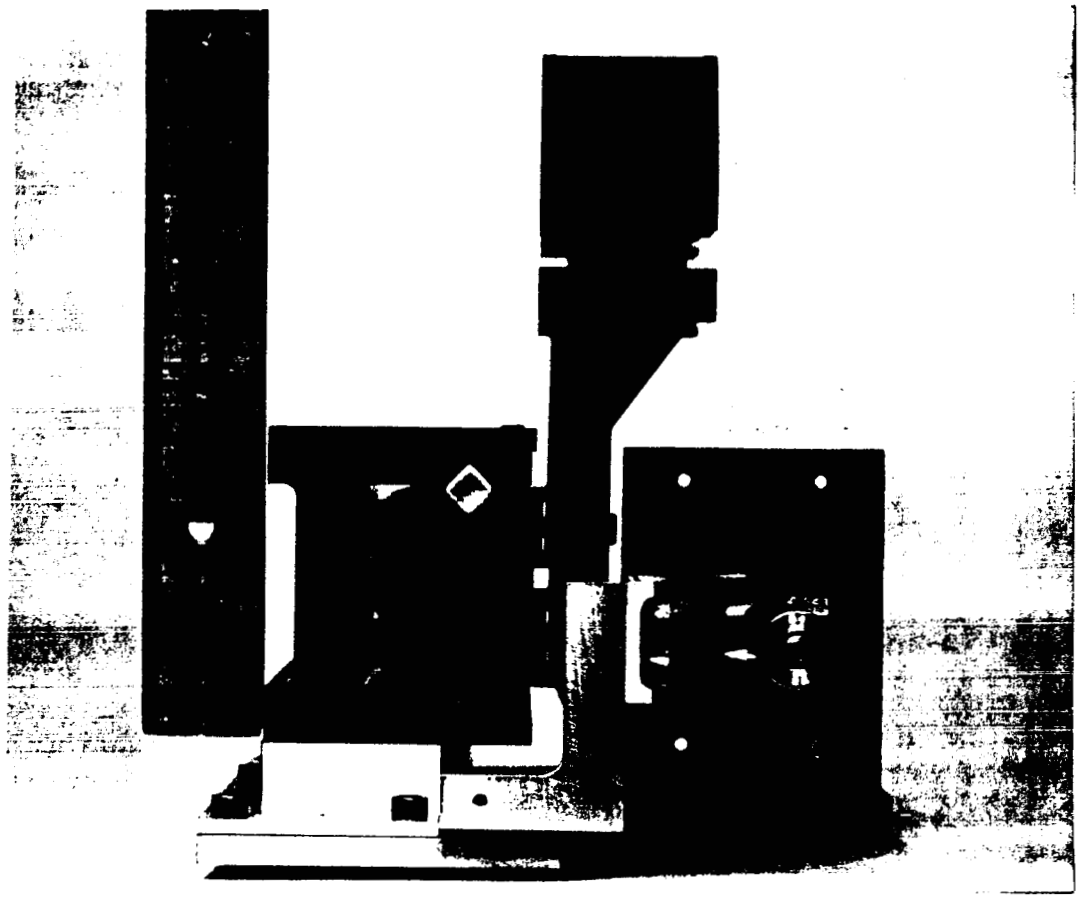

Figure 2: *Gripper (end view)*

yielding the relation

$$k_b \left(\frac{v}{rad - s}\right) = k_i \left(\frac{N - m}{A}\right). \tag{2.5}$$

In all DC permanent magnet motors there exists a ripple torque caused by the nonuniformity of the magnetic field. Thus the torque constant k_i is a function of the angular position of the rotor, and therefore periodic with period 2π. This periodic torque can effect the performance of the system, however, due to the high gear ratios being used, the effect is negligible.

Applying D'Alembert's law at the motor output, and Kirchhoff's voltage law to the circuit model of the motor, the equations for the motor are as follows:

$$J_m \dot{\omega}_m(t) = T_m(t) - T_L(t) - B_m \omega_m(t) \tag{2.6}$$

$$L_a \dot{i}_a(t) = e_a(t) - R_a i_a(t) - e_b(t) \tag{2.7}$$

where the coulomb friction, T_f, is included in the load torque, $T_L(t)$.

Selected for the actuation, the TRW 5A540-10 MM Planetary Gearmotor is manufactured with gears inside the motor housing. The gearing has the effect of decreasing

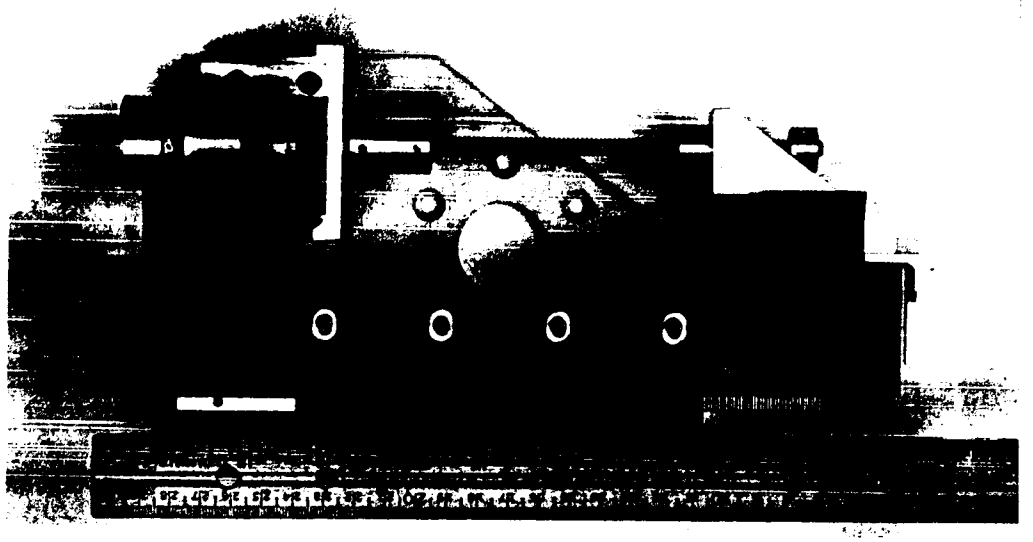

Figure 3: *Gripper (top view)*

the angular velocity and increasing the torque. The gear ratio is 27.94 and the minimum efficiency is 0.6. A summary of the other constants and their values for this motor can be found in Table 2.1. Motor variables are summarized in Table 2.2.

constant	definition	value
R_a	armature resistance	25.2 Ω
L_a	armature inductance	7.2 mH
k_i	torque constant	0.0247 $N-m/A$
k_b	back emf constant	0.0247 $V/rad/s$
J_m	rotor inertia	3.67×10^{-7} $kg-m^2$
B_m	viscous friction	0.0 $N-m/rad/s$
T_f	coulomb friction	0.0028 $N-m$

Table 2.1 *Motor Constants*

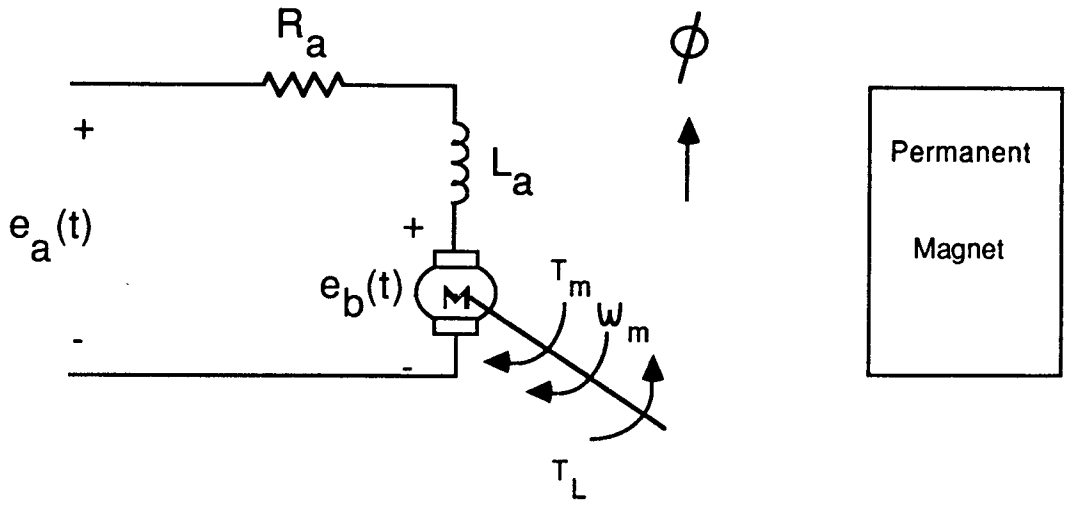

Figure 4: *Motor Model*

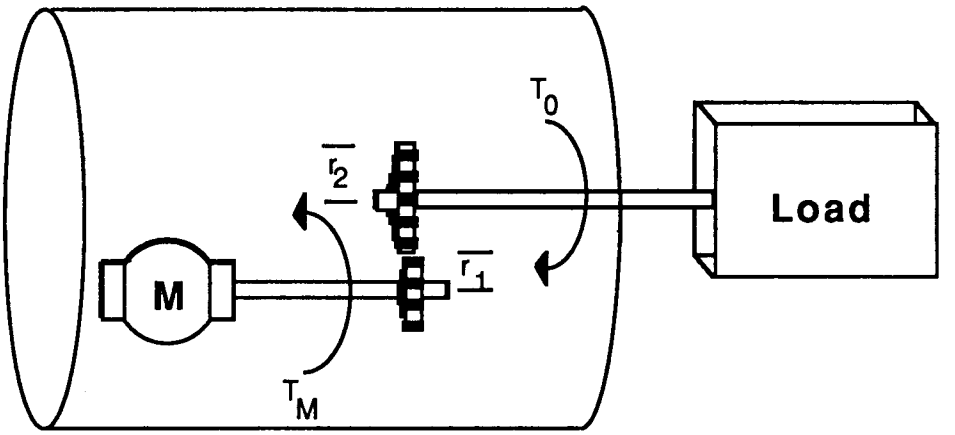

Figure 5: *Motor with Internal Gears*

variable	definition
$e_a(t)$	control voltage
$i_a(t)$	armature current
$e_b(t)$	back emf
$\omega_m(t)$	angular velocity
$T_m(t)$	motor torque
$T_L(t)$	load torque

Table 2.2 *Motor Variables*

A problem with the motor model developed above is that it gives the equations for torque and angular velocity without internal gears. These equations must be modified to account for gear effects.

Ideal gears are initially assumed in the derivation. A gear is termed ideal if it has no

moment of inertia, no stored energy, no friction, and a perfect meshing of teeth.

Let $f_c(\cdot)$ denote the contact force where the gears mesh and $N = r_1/r_2$ the gear ratio. From equation (2.6), with $T_L(t) = r_1 f_c(t)$, the equation for the motor and attached gear is

$$J_m\dot{\omega}_m(t) = T_m(t) - r_1 f_c(t) - B_m\omega_m(t) \tag{2.8}$$

also

$$T_o(t) = r_2 f_c(t) \tag{2.9}$$

Combining these two equations, and using the geometrical equality $\omega_m(t) = N\omega_o(t)$, gives

$$N^2 J_m\dot{\omega}_o(t) = NT_m(t) - T_o(t) - N^2 B_m\omega_o(t). \tag{2.10}$$

Of course, in reality the gears are not ideal. To help account for this, an efficiency term, ϵ, is included in the equation as follows

$$N^2 J_m\dot{\omega}_o(t) = \epsilon NT_m(t) - T_o(t) - N^2 B_m\omega_o(t) \tag{2.11}$$

constant	definition	value
$\bar{k}_i = \epsilon N k_i$	torque constant	$0.4141\ N-m/A$
$\bar{k}_b = N k_b$	back emf constant	$0.6901\ V/rad/s$
$\bar{J}_m = N^2 J_m$	rotor inertia	$2.9 \times 10^{-4}\ kg-m^2$
$\bar{B}_m = N^2 B_m$	viscous friction	

Table 2.3 *Equivalent Motor Constants*

By using the equivalent constants defined in Table 2.3 the adapted motor equations become

$$\bar{J}_m\dot{\omega}_o(t) = \bar{T}_m(t) - T_L(t) - \bar{B}_m\omega_o(t) \tag{2.12}$$

$$L_a\dot{i}_a(t) = e_a(t) - R_a i_a(t) - \bar{e}_b(t) \tag{2.13}$$

$$\bar{T}_m(t) = \bar{k}_i i_a(t) \tag{2.14}$$

$$\bar{e}_b(t) = \bar{k}_b\omega_o(t) \tag{2.15}$$

The transmission mechanism used is an acme screw. The acme screw serves to transform rotary motion of the motor to linear motion needed to move the fingers. A screw with a small lead angle, $\ell = 1.6\ mm$, was used so that larger finger tip forces could be developed while using a smaller motor. As a trade-off, the maximum velocity attained during opening and closing is lower. Another benefit of having a small lead angle is that the screw is self locking under reasonable load conditions. This is an important feature since it will allow the end effector to hold objects without using power. This property helps to eliminate problems created because of poor heat dissipation in space.

Used to link the motion of the fingers, the rack and pinion gear's effect is to move the fingers at the same velocity in opposite directions. The model, which is developed

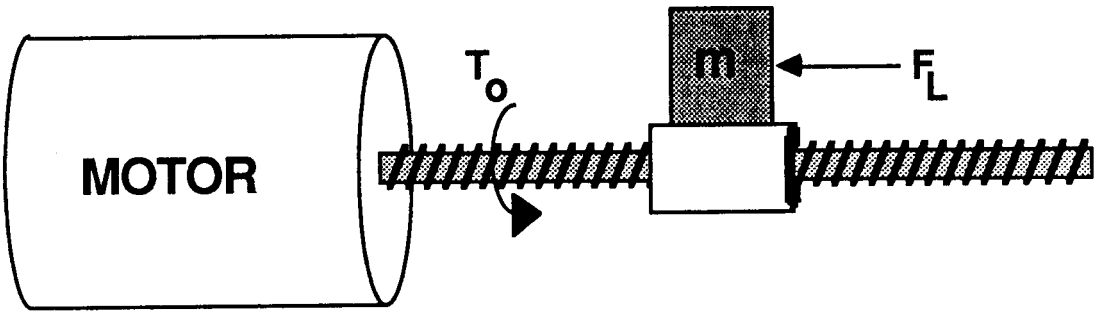

Figure 6: *System Diagram*

for the force and velocity of one of the fingers, is effected only by the efficiency of this gear.

The finger assembly is modeled as a rigid body since operating forces are far below the magnitude necessary to result in significant deflections of the aluminum body. Because the motion is strictly linear the moving parts in the finger assembly are treated as a point mass located at the nut. Table 2.4 lists the moving parts and their weights.

Since the errors due to backlash caused by the gears (the motor's internal gears, the acme screw, and the rack and pinion) will be within desired positioning accuracy of $\pm 0.25cm$, they can be ignored in the model development. Position control will be employed only to achieve an approximate desired finger opening; force control will be used upon encountering an object. Therefore, a course positioning scheme will be sufficient.

part	weight
long finger	0.568 *kgs*
short finger	0.477 *kgs*
bearings	0.091 *kgs*

Table 2.4 *Weight of Moving Gripper Parts*

The last step in the model development is to relate output force at the fingers and output velocity of the fingers to the input armature voltage.

Assume initially that the screw is ideal. For an ideal screw, the translation from angular velocity of the motor output shaft to linear velocity of the fingers is

$$V_L(t) = \frac{\ell}{2\pi}\omega_o(t) \tag{2.16}$$

and the transformation from torque to force is

$$F_c(t) = \frac{2\pi}{\ell}T_c(t) \tag{2.17}$$

where $T_c(\cdot)$and $F_c(\cdot)$ denote the coupling torque and force respectively between the screw and the nut. Then developing the equations as before

$$\bar{J}_m\dot{\omega}_o(t) = \bar{T}_m(t) - T_c(t) - \bar{B}_m\omega_o(t) \tag{2.18}$$

$$F_L(t) = F_c(t) - m\dot{V}_L(t) \tag{2.19}$$

Combining these equations and applying the screw equations (2.16) and (2.17) yields

$$F_L(t) = (\frac{2\pi}{\ell})\bar{T}_m - ((\frac{2\pi}{\ell})^2\bar{J}_m + m)\dot{V}_L(t) - (\frac{2\pi}{\ell})^2\bar{B}_m V_L(t) \tag{2.20}$$

As before efficiency terms, μ and ρ, are incorporated into the model to account for the losses in the non-ideal screw and rack and pinion gears respectively. For an acme screw the efficiency is approximately 0.4, and for the rack and pinion 0.7.

$$F_L(t) = \mu\rho(\frac{2\pi}{\ell})\bar{T}_m - ((\frac{2\pi}{\ell})^2\bar{J}_m + m)\dot{V}_L(t) - (\frac{2\pi}{\ell})^2\bar{B}_m V_L(t) \tag{2.21}$$

Included in the load force, $F_L(\cdot)$, is the friction due to bearing preload which is 1.362 N. This is arrived at by estimating the preload force at 4.45 N ($\approx$ 10 lbs), and the coefficient of friction for the roller bearings at 0.3.

Taking the Laplace transform of equations (2.13)-(2.16) and (2.21), after some algebraic manipulation yields

$$V_L(s) = \frac{\mu\rho(\frac{\ell}{2\pi})\bar{k}_i e_a(s)}{(\bar{J}_m + (\frac{\ell}{2\pi})^2 m)L_a s^2 + ((\bar{J}_m + (\frac{\ell}{2\pi})^2 m)R_a + L_a\bar{B}_m)s + (R_a\bar{B}_m + \mu\rho\bar{k}_i\bar{k}_b)} - \frac{(\frac{\ell}{2\pi})^2(L_a s + R_a)F_L(s)}{(\bar{J}_m + (\frac{\ell}{2\pi})^2 m)L_a s^2 + ((\bar{J}_m + (\frac{\ell}{2\pi})^2 m)R_a + L_a\bar{B}_m)s + (R_a\bar{B}_m + \mu\rho\bar{k}_i\bar{k}_b)} \tag{2.22}$$

$$T_m(s) = \frac{\bar{k}_i((\bar{J}_m + (\frac{\ell}{2\pi})^2 m)s + \bar{B}_m)e_a(s)}{(\bar{J}_m + (\frac{\ell}{2\pi})^2 m)L_a s^2 + ((\bar{J}_m + (\frac{\ell}{2\pi})^2 m)R_a + L_a\bar{B}_m)s + (R_a\bar{B}_m + \mu\rho\bar{k}_i\bar{k}_b)} + \frac{\bar{k}_i\bar{k}_b(\frac{\ell}{2\pi})F_L(s)}{(\bar{J}_m + (\frac{\ell}{2\pi})^2 m)L_a s^2 + ((\bar{J}_m + (\frac{\ell}{2\pi})^2 m)R_a + L_a\bar{B}_m)s + (R_a\bar{B}_m + \mu\rho\bar{k}_i\bar{k}_b)} \tag{2.23}$$

Found in appendix A are the magnitude Bode plots of the model transfer function for position, velocity and force. Obtained from NASA by measuring the *gripper* response to a series of incremented sine waves, the true bode plot for position are found in appendix B. The accuracy of the true Bode plot for frequency greater than 8 rad/s is extremely poor due to backlash in the system. This will not effect performance since the fingers will not be expected to make rapid changes in direction. The actual bode plot reveals that for the range of operation the system only second order dynamics are evident. This implies that the third order dynamics cause by the nonzero inductance can be ignored and thus it can be assumed that the inductance is zero. The magnitude Bode plots of the transfer function for position, and velocity with inductance equal to zero have been superimposed on the third order model plots found in appendix A.

3 State Space Realization

From the transfer function for the velocity of the fingers comes the position transfer function (assuming $L_a = 0$):

$$P(s) = \frac{\mu\rho(\frac{\ell}{2\pi})\bar{k}_i e_a(s)}{s((\bar{J}_m + (\frac{\ell}{2\pi})^2 m)R_a s + (R_a\bar{B}_m + \mu\rho\bar{k}_i\bar{k}_b))} - \frac{(\frac{\ell}{2\pi})^2 R_a F_L(s)}{s((\bar{J}_m + (\frac{\ell}{2\pi})^2 m)R_a s + (R_a\bar{B}_m + \mu\rho\bar{k}_i\bar{k}_b))} \tag{3.1}$$

Rewritten to simplify notation as

$$P(s) = \frac{c_1 e_a(s) - c_2 F_L(s)}{s(s^2 + c_3 s + c_4)}. \tag{3.2}$$

This transfer function describes a linear time invariant system which has two inputs, armature voltage, $e_a(\cdot)$, and load torque, $F_L(\cdot)$, one output, finger position, $P(\cdot)$. The minimal realization has two states, finger position, $P(\cdot)$, and finger velocity, $V_L(\cdot)$. In state space form, the minimal system is written as

$$\begin{cases} \dot{\mathbf{x}}(t) = \mathbf{A}\mathbf{x}(t) + \mathbf{B}\mathbf{u}(t) \\ y(t) = \mathbf{C}\mathbf{x}(t) \end{cases} \tag{3.3}$$

where

$$\mathbf{A} = \begin{pmatrix} 0 & 1 \\ 0 & -c_3 \end{pmatrix} \tag{3.4}$$

$$\mathbf{B} = \begin{pmatrix} 0 & 0 \\ c_1 & -c_2 \end{pmatrix} \tag{3.5}$$

$$\mathbf{C} = \begin{pmatrix} 1 & 0 \end{pmatrix}. \tag{3.6}$$

Note that since this realization is minimal, it is both controllable and observable.

4 Optimal Position Controller (Bang Bang Control)

It is desirable to determine the control which moves the fingers from the initial state (position, velocity), $\mathbf{x}_0 = (\,x_0 \quad 0\,)'$, to the desired final state, $\mathbf{x}_f = (\,x_f \quad 0\,)'$, in minimum time. Such problems have been extensively studied in optimization theory. One solution to the minimum time problem follows from the well known Pontryagin Minimum Principle (PMP). The necessary conditions derived from the PMP for linear time invariant systems are detailed below [3].

4.1 Problem Statement

Given a completely controllable dynamical system

$$\dot{\mathbf{x}}(t) = \mathbf{A}\mathbf{x}(t) + \mathbf{B}\mathbf{u}(t) \tag{4.1}$$

such that the components $u_1(t), u_2(t), \ldots u_r(t)$ of $\mathbf{u}(t)$ are constrained in magnitude by the relation

$$|u_j(t)| \leq M_j \qquad j = 1, 2, \ldots \tag{4.2}$$

and that at the initial time $t_0 = 0$, the initial state of the system is $\mathbf{x}_0 \triangleq \mathbf{x}(t_0)$, find a control $\mathbf{u}^*(\cdot)$ that transfers the system from $\mathbf{x}_0$ to $\mathbf{x}_f$ in minimum time. This control is called the time optimal control.

4.2 Necessary Conditions

Assume that a time optimal control, $\mathbf{u}^*(t)$, exists that transfers the initial state $\mathbf{x}_0$ to $\mathbf{x}_f$. Let $\mathbf{x}^*(t)$ denote the trajectory of the system corresponding to $\mathbf{u}^*(t)$, originating at $\mathbf{x}_0$ at $t_0 = 0$, and hitting $\mathbf{x}_f$ in the minimum time, T^*. Then there exists a corresponding costate vector $\mathbf{p}^*(t)$ such that:

1. $\mathbf{x}^*(t)$ and $\mathbf{p}^*(t)$ are solutions of the canonical equations

$$\dot{\mathbf{x}}^*(t) = \frac{\partial H}{\partial \mathbf{p}^*}(\mathbf{x}^*(t), \mathbf{u}^*(t), \mathbf{p}^*(t)) = \mathbf{A}\mathbf{x}^*(t) + \mathbf{B}\mathbf{u}^*(t) \tag{4.3}$$

$$\dot{\mathbf{p}}^*(t) = -\frac{\partial H}{\partial \mathbf{x}^*}(\mathbf{x}^*(t), \mathbf{u}^*(t), \mathbf{p}^*(t)) = -\mathbf{A}'\mathbf{p}^*(t) \tag{4.4}$$

with boundary conditions

$$\mathbf{x}^*(0) = \mathbf{x}_0, \qquad \mathbf{x}^*(T^*) = \mathbf{x}_f. \tag{4.5}$$

Called the Hamiltonian function,

$$H(\mathbf{x}(t), \mathbf{u}(t), \mathbf{p}(t)) = 1 + < \mathbf{A}\mathbf{x}(t) + \mathbf{B}\mathbf{u}(t), \mathbf{p}(t) > \tag{4.6}$$

for linear time invariant systems.

2. The relation

$$H(\mathbf{x}^*(t), \mathbf{u}^*(t), \mathbf{p}^*(t)) \leq H(\mathbf{x}^*(t), \mathbf{u}(t), \mathbf{p}^*(t)) \tag{4.7}$$

holds for all admissible $\mathbf{u}(t)$ and for $t \in [0, T^*]$. From equation (4.7), this implies

$$\langle \mathbf{B}'\mathbf{p}^*(t), \mathbf{u}^*(t) \rangle \leq \langle \mathbf{B}'\mathbf{p}^*(t), \mathbf{u}(t) \rangle \tag{4.8}$$

holds for all admissible $\mathbf{u}(t)$ and for $t \in [0, T^*]$. Clearly, $< \mathbf{B}'\mathbf{p}^*(t), \mathbf{u}(t) >$ is minimized by

$$u_j^*(t) = -Msgn(\mathbf{b}_j'\mathbf{p}^*(t)), \tag{4.9}$$

where $\mathbf{b}_j$ denotes the j^th column of $\mathbf{B}$.

3. The relation

$$H(\mathbf{x}^*(t), \mathbf{u}^*(t), \mathbf{p}^*(t)) = 0 \tag{4.10}$$

holds for all $t \in [0, T^*]$.

Thus it has been shown that if an optimal control exists, it may only take on values $\pm M_j \ \forall j$. The second input, $F_L(\cdot)$, is depend on the particular task and thus cannot be set optimally. For the first input, $e_a(\cdot)$, the set of feasible controls is practically limited by the maximum armature voltage, 24 V.

4.3 Switching Curves

The necessary conditions do not contain any explicit information regarding either the initial costate, $\mathbf{p}^*(0)$, or the terminal costate, $\mathbf{p}^*(T^*)$. However, from equation (4.6) and (4.10) it follows that the costate, $\mathbf{p}^*(t)$, must be a nonzero vector. That is

$$\mathbf{p}^*(t) \neq \mathbf{0} \quad \forall t \in [0, T^*]. \tag{4.11}$$

The *switching times* of the control voltage can be found by finding the time at which

$$\mathbf{b}_1' \mathbf{p}^*(t) = c1 p_2(t) = 0. \tag{4.12}$$

Solving equation (4.4) for the costate yields:

$$p_1^*(t) = p_1^*(0) = constant \tag{4.13}$$

$$p_2^*(t) = (\frac{1}{c} 3 p_1^*(0) + p_2^*(0)) \exp c3 - \frac{1}{c} 3 p_1^*(0) \tag{4.14}$$

Since $p_1^*(\cdot)$ is constant, and $p_2^*(\cdot)$ is monotonic in t, the control voltage changes signs at most once. Without information on the initial or final costate, the *switching time* cannot be determined from these equations.

Disregarding the question of determining the initial or final costate, investigate which among the feasible controls just obtained steers the given initial state to the final state. Assumed here is that the load force will be essentially constant and equal to the internal frictional force. This will be the general case when operating in the position control mode. Solving equation (4.1) yields

$$x_1(t) = x_0 + \frac{c1u(t) - c2F_L}{c} 3t + \frac{c1u(t) - c2F_L}{c} 3^2(1 - exp - c3t) \tag{4.15}$$

$$x_2(t) = -\frac{c1u(t) - c2F_L}{c} 3(1 - exp - c3t) \tag{4.16}$$

By substituting for $u(\cdot)$ in equations (4.15) and (4.16), find which of the feasible controls achieves the desired goal. This control is the optimal control.

Substituting the model parameters from section 1, it can be seen that the switching time is within the position error margins of $\pm .25cm$.

5 Hardware Implementation

Chosen to implement the controller in real time, the Mac II has been equipped with a MacAdios board for D/A and A/D conversions. To boost the power in the control signal, an amplifier was built using the Burr-Brown high power operational amplifier (Figure 9). The decision to use the Mac II was based on the need for a *design environment* that would facilitate rapid design and testing of control algorithms. In addition the mouse/icon oriented environment allows new users to come up to speed with a minimum of training.

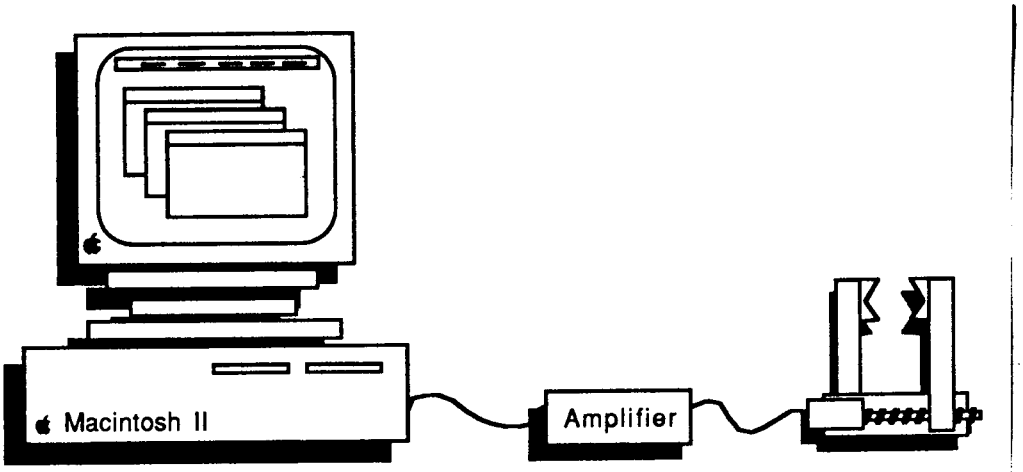

Figure 7: *Hardware Flow Diagram*

The time optimal position controller has been implimented. The controller can position to within $\pm.25$ cm of the desired position without overshoot. The top velocity can be set arbitrarily between the maximum value, approximately 1.25 cm/s, and 0 cm/s.

Since fingers equipped with the full array of strain gauges have not yet been delivered by NASA, the force controller currently running receives force information from only one strain gauge on each finger and thus is not able to compute the grip points or finger torques. Any finger force between 0 N and approximately 6.0 N can be maintained. Addressing the problem of hitting an unexpected obstacle, the hybrid force/position controller stops if a prespecified force is achieved during positioning.

5.1 Future Plans

Impeded by disagreements in the initial design environment and delays in delivering the mechanical hardware, progress is slow and there is still much work to be done. The major focuses are detailed below.

1. Upon receipt of the fingers equipped with the complete array of strain gauges, an algorithm which determines grip points an finger torques will be tested.

2. Once the control algorithms have been perfected, they will be programmed onto a dedicated signal processing chip and the Mac II will be used only for higher level processing, leaving the low level calculations and commands to the signal processing chip.

References

[1] J. Vranish, "Wheatstone bridge,". Details the force sensor design.

[2] K. Ogata, *Modern Control Engineering.* Elglewood Cliffs, NJ: Prentice Hall, 1970.

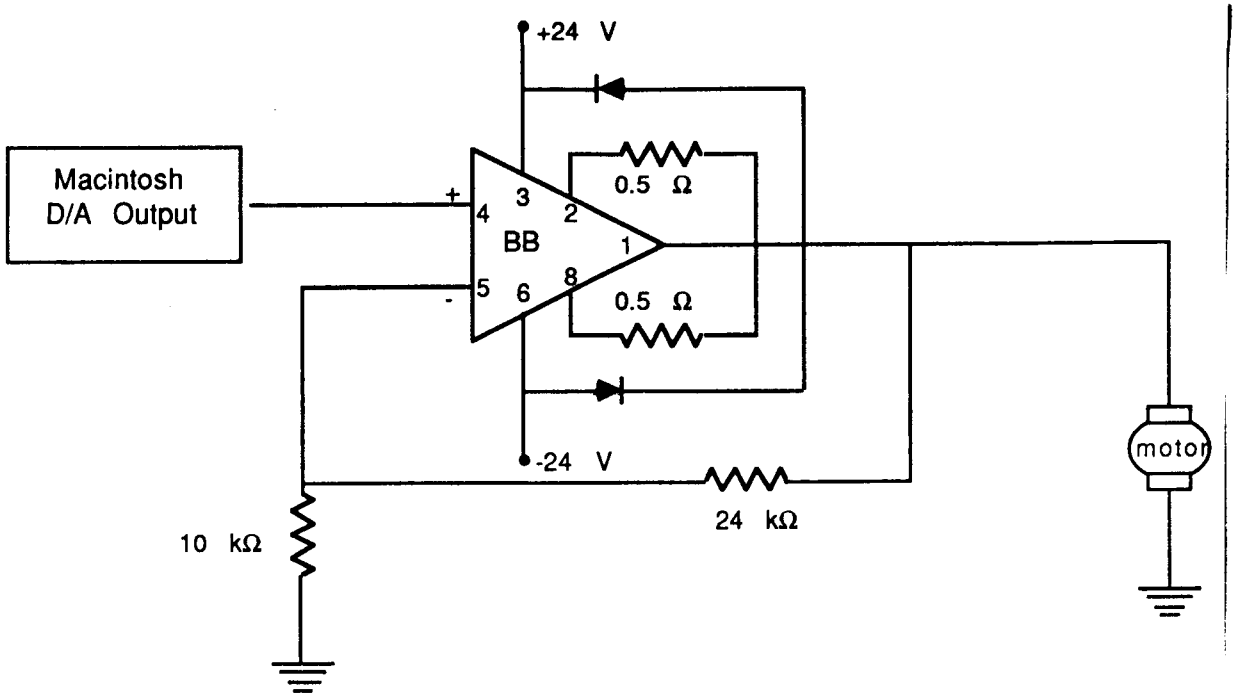

Figure 8: *Amplifier Diagram*

[3] M. Athans and P. Falb, *OPTIMAL CONTROLS: An Introduction to the Theory and It's Applications.* New York, NY: McGraw-Hill, 1966.

[4] C. Close and D. Frederic, *Modeling and Analysis of Dynamic Systems.* Boston, MA: Houghton Mifflin Company, 1978.

[5] C. Chen, *Linear Systems Theory and Design.* New York, NY: Holt, Reinhard and Winston, 1984.

[6] Electrocraft Corporation, ed., *DC Motors, Speed Controls, Servo Systems.* Elmsfor, NY: Pergamon Press, fifth ed., 1980.

A Model Bode Plots: position, velocity, force

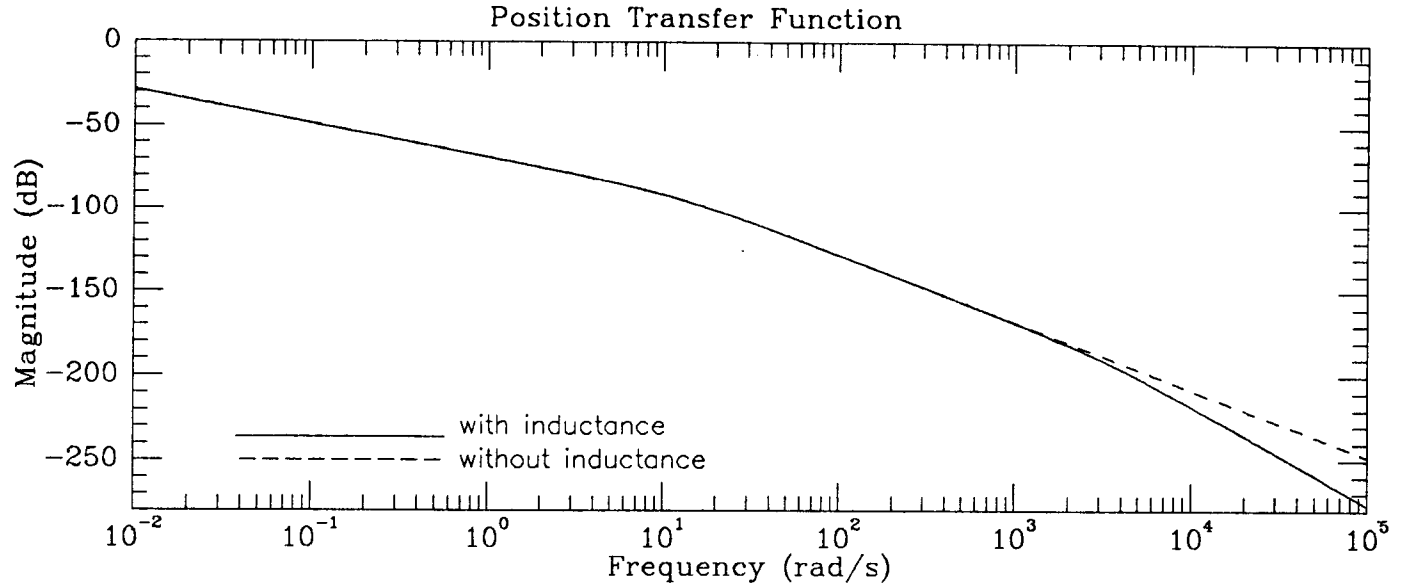

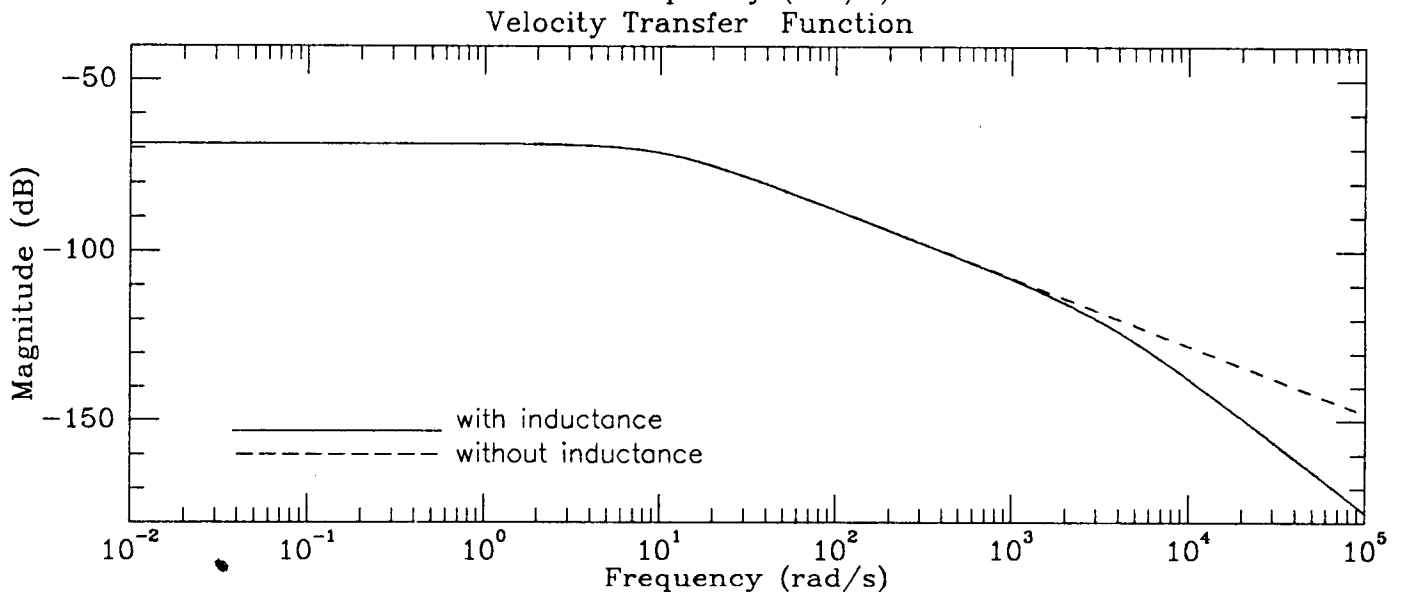

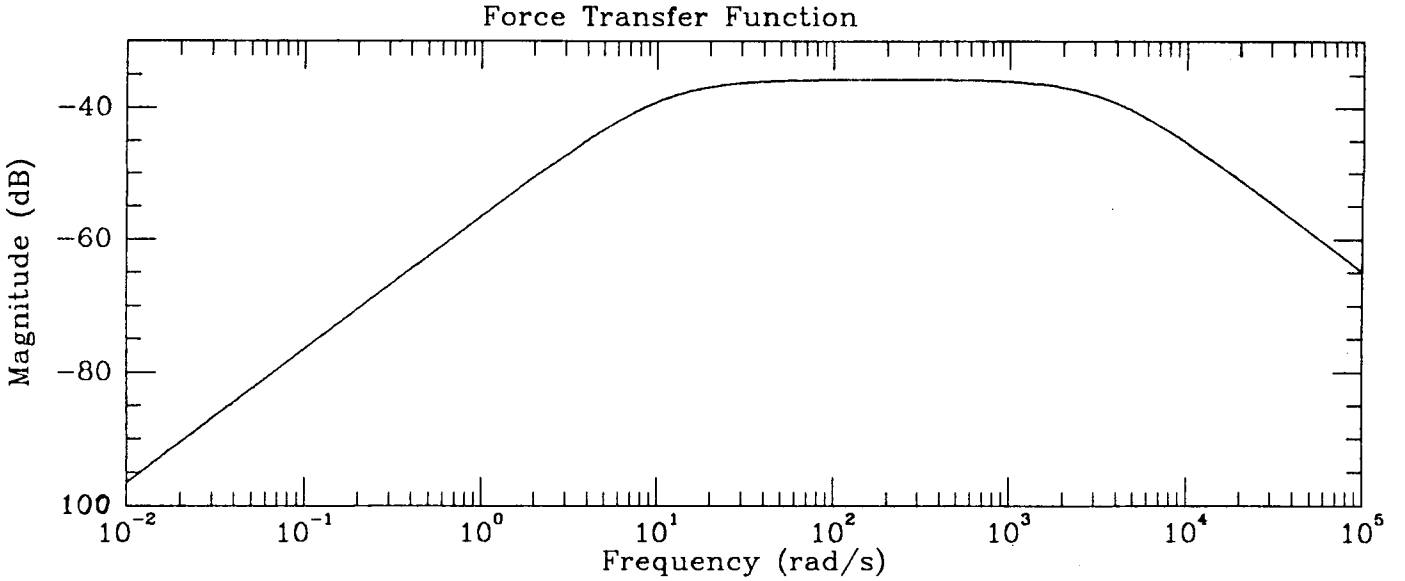

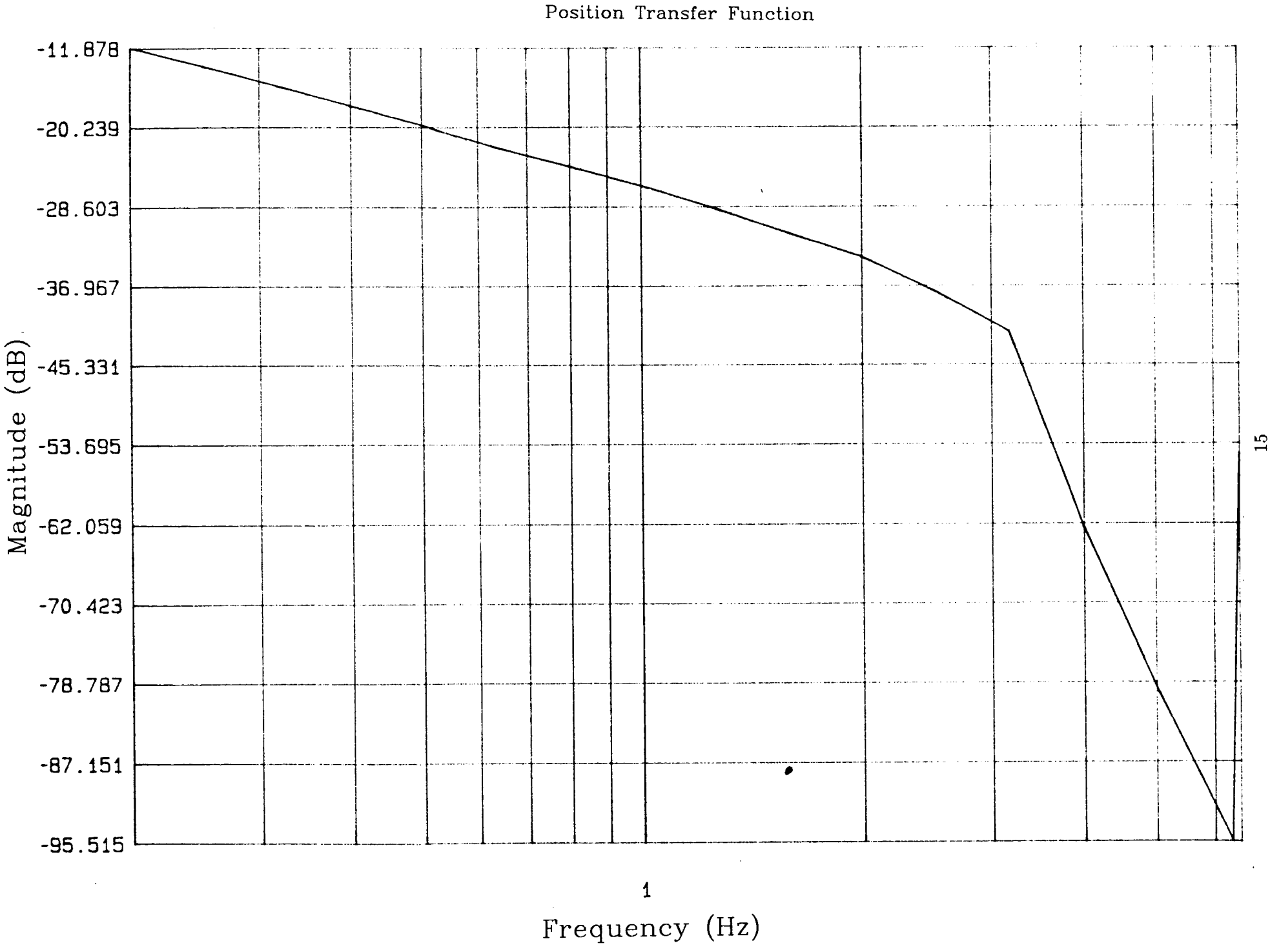
Position Transfer Function
-11.878
-20.239
-28.603
-36.967
-45.331
-53.695
-62.059
-70.423
-78.787
-87.151
-95.515
Magnitude (dB)
1
Frequency (Hz)
15